

Autonomous Surface Vehicle Free-Rotating Wingsail Section Design and Configuration Analysis

Gabriel Hugh Elkaim*

University of California, Santa Cruz, Santa Cruz, California 95064

DOI: 10.2514/1.27284

The Atlantis Project is a wing-based autonomous sailing vessel, based on a Prindle-19 catamaran, that has demonstrated line following under automatic control to an accuracy of better than 0.3 meters. This work details both the design of the wing section and the configuration analysis for a free-rotating, aerodynamically actuated wingsail that is used as the main propulsion system. Based on numerical airflow analysis using PANDA and XFOIL of the low Reynolds number aerodynamic performance, a symmetric section with a small trailing-edge flap is used in a conventional arrangement (tail behind the main section). This allows efficient sailing to both port and starboard, as well as retaining high-lift coefficients for broad reaches. The inability of the flow to withstand adverse pressure gradients at the typically low Reynolds number causes separation with flap deflection, thus necessitating a narrow-chord flap that is deflected through a large angle for high-lift applications. The designed section has a $C_{L_{max}}$ of 1.8 at a Reynolds number of 229,000, and a flap deflection of 45 deg. The wing section is 21% thick, with a 13% plain flap to achieve this maximum lift coefficient. Four different configurations are evaluated for stability and swept radius (the farthest distance that the entire wingsail reaches as it rotates about the mast). The configurations evaluated are 1) conventional, 2) canard, 3) flying wing, and 4) free-floating canard. The canard and the flying wing cannot be made passively stable with a high coefficient of lift, whereas the free-floating canard and the conventional configuration achieve the stability criteria. The free-floating canard has a larger swept radius and has issues with stall stability that are not covered by this simplified analysis, thus the conventional configuration (tail behind the wing) is determined best for this application.

Nomenclature

\mathcal{AR}	= aspect ratio
b	= wing semispan
C_D	= drag coefficient
C_L	= lift coefficient
C_M	= pitching moment coefficient
C_p	= section pressure coefficient
c	= section chord
D	= drag, N
d	= distance from pivot point to trimming surface
L	= lift, N
M	= pitching moment about quarter chord, N · m
Re	= Reynolds number
R_s	= swept radius
S	= area
sm	= distance from pivot point to main wing aerodynamic center
x	= chordwise distance, leading to trailing edge
y	= spanwise distance, root to tip
α	= angle of attack
δ_f	= flap deflection
Λ_s	= wing sweep angle
λ	= wing taper ratio

Subscripts

c	= canard
f	= flap
free	= free-floating canard
max	= maximum

qc	= quarter chord
T	= tail
W	= wing
0	= offset
\oplus	= pivot point

I. Introduction

THE Atlantis, pictured in Fig. 1, is an unmanned, autonomous, Global Positioning System (GPS) guided, wingsailed catamaran. The Atlantis has demonstrated an advance in control precision of a wind-propelled marine vehicle to an accuracy of better than 1 m. This quantitative improvement in control enables new applications, including unmanned station-keeping for navigation or communication purposes, autonomous “dock-to-dock” transportation capabilities, emergency “return unmanned” functions, precision marine science monitoring [1], and many others still to be developed. The prototype is based on a modified Prindle-19 light catamaran.

The wind-propulsion system is a rigid wingsail mounted vertically on bearings to allow free rotation in azimuth about a stub mast (the design of which is detailed in this paper). Aerodynamic torque about the stub mast is trimmed using a flying tail mounted on booms joined to the wing. This arrangement allows the wingsail to automatically attain the optimum angle to the relative wind, and weather vane into gusts without inducing large heeling moments. Modern airfoil design allows for an increased lift-to-drag ratio L/D over a conventional sail, thus providing thrust while substantially reducing the overturning moment.

The system architecture is based on distributed sensing and actuation with a high-speed digital serial bus connecting the various modules together [2]. Sensors are sampled at 100 Hz, and a central guidance navigation and control computer performs the required estimation and control tasks at 5 Hz. This bandwidth has been demonstrated to be capable of precise control.

The sensor system uses differential GPS (DGPS) for position and velocity measurements, augmented by a low-cost attitude system based on accelerometer and magnetometer triads [3], which are combined to create a “synthetic” position sensor located at the center of gravity rather than at the GPS antenna location.

Received 14 August 2006; accepted for publication 22 April 2008. Copyright © 2008 by the American Institute of Aeronautics and Astronautics, Inc. All rights reserved. Copies of this paper may be made for personal or internal use, on condition that the copier pay the \$10.00 per-copy fee to the Copyright Clearance Center, Inc., 222 Rosewood Drive, Danvers, MA 01923; include the code 0021-8669/08 \$10.00 in correspondence with the CCC.

*Assistant Professor, Department of Computer Engineering, 1156 High Street. AIAA Member.



Fig. 1 Photograph of Atlantis.

Previous experimental trials recorded sensor and actuator data intended to excite all system modes but while under electric motor propulsion. A system model was assembled using Observer/Kalman System Identification techniques [4]. A linear quadratic Gaussian (LQG) controller was designed using the identified model, using an estimator based on the experimental noise statistics. Experimental tests were run to sail on a precise track through the water, in the presence of currents, wind, and waves.

To validate the performance of the controllers and all-up system, closed-loop control experiments were performed. These tests were intended to verify that the closed-loop controllers were capable of precise line following with the increased disturbances due to the wingsail propulsion. No modifications were made to the LQG controller design, and the tests were run on a day with approximately 12 kt (or 6 m/s) of wind, with gusts up to the 20 kt (or 10 m/s) range [5].

The Atlantis proved to be capable of sailing to within 25 deg of the true wind direction, though performance degraded rapidly above 40 deg. Figure 2 presents a close-up of the first path of regulated control and looks at the cross-track error, azimuth error, and velocities while tracking a line. Note that the dark line in the top of the boat speed graph (bottom panel) is the relative wind speed, and it shows large variations.

The mean of the cross-track error is less than 3 cm, and the standard deviation is less than 30 cm; note that this is the sailboat technical error (the sailing analog of flight technical error) defined as the difference between the measured position (using DGPS) and the commanded sailboat position. Previous characterization of the Coast Guard differential GPS receiver indicated that the navigation sensor error is approximately 36 cm, thus the total system error is less than 1 m [2].

The most visibly unique aspect of the Atlantis project is the wingsail propulsion system, as shown in Fig. 3. This paper details the design evolution that results in the unique configuration of the wingsail, both in section and configuration. The design considerations and goals are 1) equivalent performance to the original sail system, 2) low actuation force, and 3) the ability to precisely control the resulting system. A sloop rig sail can achieve a

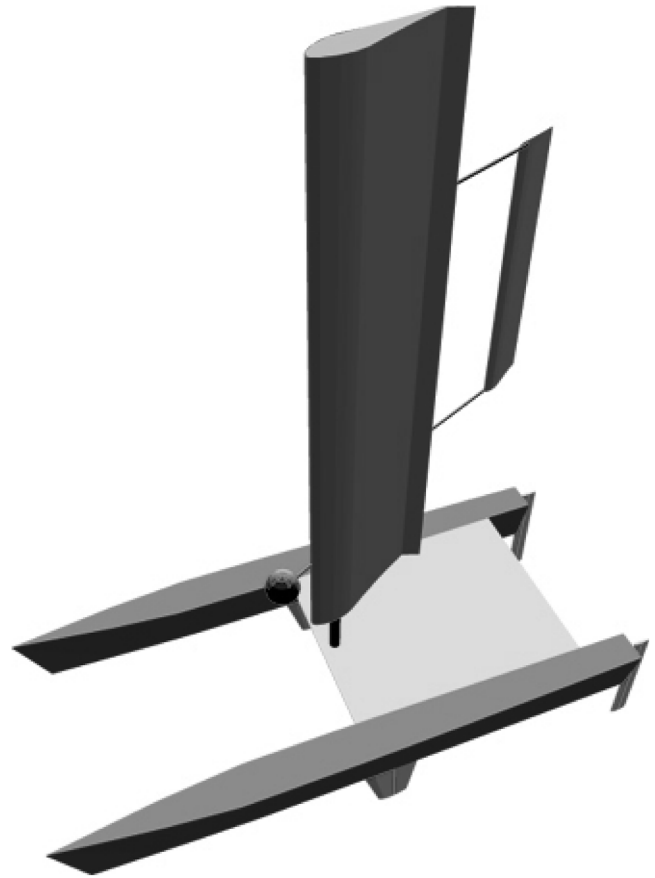


Fig. 3 Engineering model of the Atlantis.

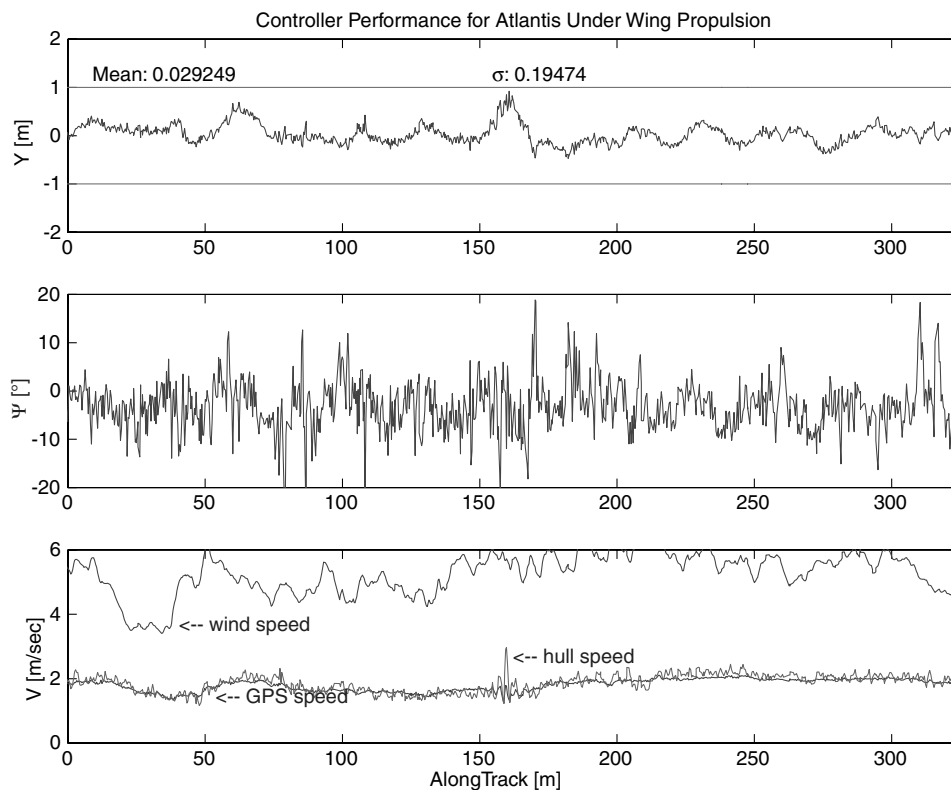


Fig. 2 Sailing path errors, cross-track error (top), heading error (center), and boat and wind velocities (bottom).

maximum lift coefficient of 0.8 if the jib and sail are perfectly trimmed. Realistically, an operating maximum lift coefficient of 0.6 is more likely. The design goal of the Atlantis wing is to achieve a maximum lift coefficient of 1.8. Because this allows the wing to generate 3 times the force of an equivalently sized sail, the wing area is reduced to one-third of the area of the original sails. Because the drag characteristics of the wing are much improved, the performance of the wingsailed catamaran should be superior to the original configuration. At worst, the wing will yield equivalent performance.

Motivated by the goal of autonomous operation, the actuation of the sail must be simple. In the case of a conventional sail, this would be challenging in terms of actuator cost and power required, as the forces required are quite large. Additionally, the complex nature of the aerodynamics of a cloth sail makes any sort of precise control difficult to accomplish. Precision control of the catamaran requires that the disturbances generated by the propulsion system be minimized [6–9]. Fundamentally, this forces the design away from a conventional cloth sail.

Figure 4 shows the design evolution of the wingsail. The design choices are shown on the right with the choices designated by triangles, with the losing choice on the left and the winning choice on the right. The text explains the reasoning behind the choice. The steps are each detailed in later sections. The first choice is between a conventional cloth sail or a rigid wingsail, then between a symmetrical or asymmetrical section. Following the symmetry choice, an existing section and a custom-designed airfoil section are considered. With the section design complete, the next issue is to trim the wing aerodynamically or mechanically. Lastly, four possible configurations for the wing and trimming surface are considered.

The series of choices lead the design to a self-trimming wingsail with a conventional tail, using a custom-designed airfoil section for the appropriate Reynolds number. The remainder of this paper considers each choice in detail. Section II details the choices between the wing versus sail, Sec. III explains the Reynolds number effects,

Sec. IV explores the requirements for symmetry, and Sec. V details the airfoil section design. The configuration and stability analysis is discussed in Sec. VI, with the results presented in Sec. VII. Lastly, Conclusions are presented in Sec. VIII.

II. Wing Versus Sail

The final wingsail is 5.37 m tall and has a chord of 1.45 m. It is constructed in three sections: the lower section, which includes the forward electronics/ballast pod, the middle section with the tail (attached by twin booms), and the upper section. The wingsail is built entirely of marine-grade plywood covered in polyester fabric and is suspended by a spherical roller bearing at the top of the stub mast and stabilized by a needle roller bearing at the bottom of the wing. This allows the wing to rotate freely through 360 deg without significant resistance. An engineering diagram of the wing is shown in Fig. 5.

There are three main reasons to use a wing instead of a sail: 1) efficiency, 2) low actuation force, and 3) self-trimming (passive stability). A rigid wing can be far more efficient than a cloth sail, with a $C_{L_{max}}$ of 1.8 vs 0.8, though attention needs to be paid to Reynolds number effects. The lift/drag L/D ratio of the wingsail section is in the 30–100 range, whereas the L/D of the conventional sail is in the 3–5 range [10]. Further, a cloth sail suffers from aeroelastic collapse when pointed high into the wind (the sail is said to be luffing), which causes a substantial drag rise and effectively limits how high the boat can sail into the wind. A rigid wing, by contrast, suffers no aeroelastic problems; it can point straight into the wind with very little drag and no noise, effectively reefing the wing. The feathered wing–tail combination has less drag than the bare mast (see Fig. 6). This addresses the most common objection to rigid wingsails: the inability to reef the sail (or reduce the area). Note that this point is moot because the wing has far less aerodynamic load on it than the bare mast itself when feathered (tail set to 0 deg).

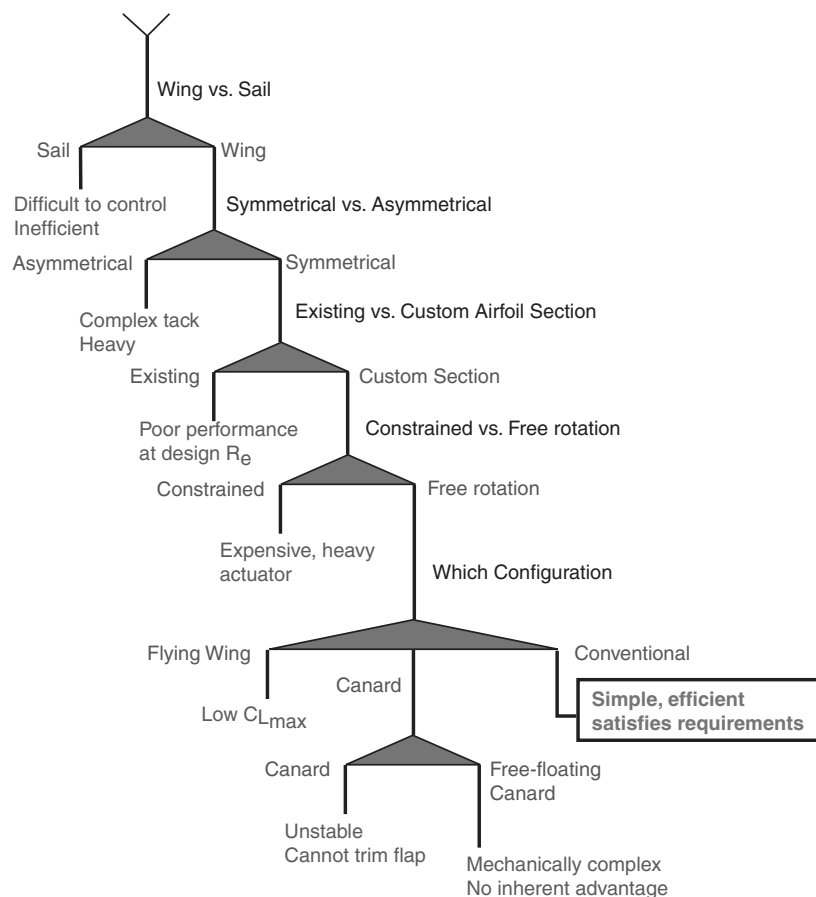


Fig. 4 Design evolution of the wingsail propulsion system.

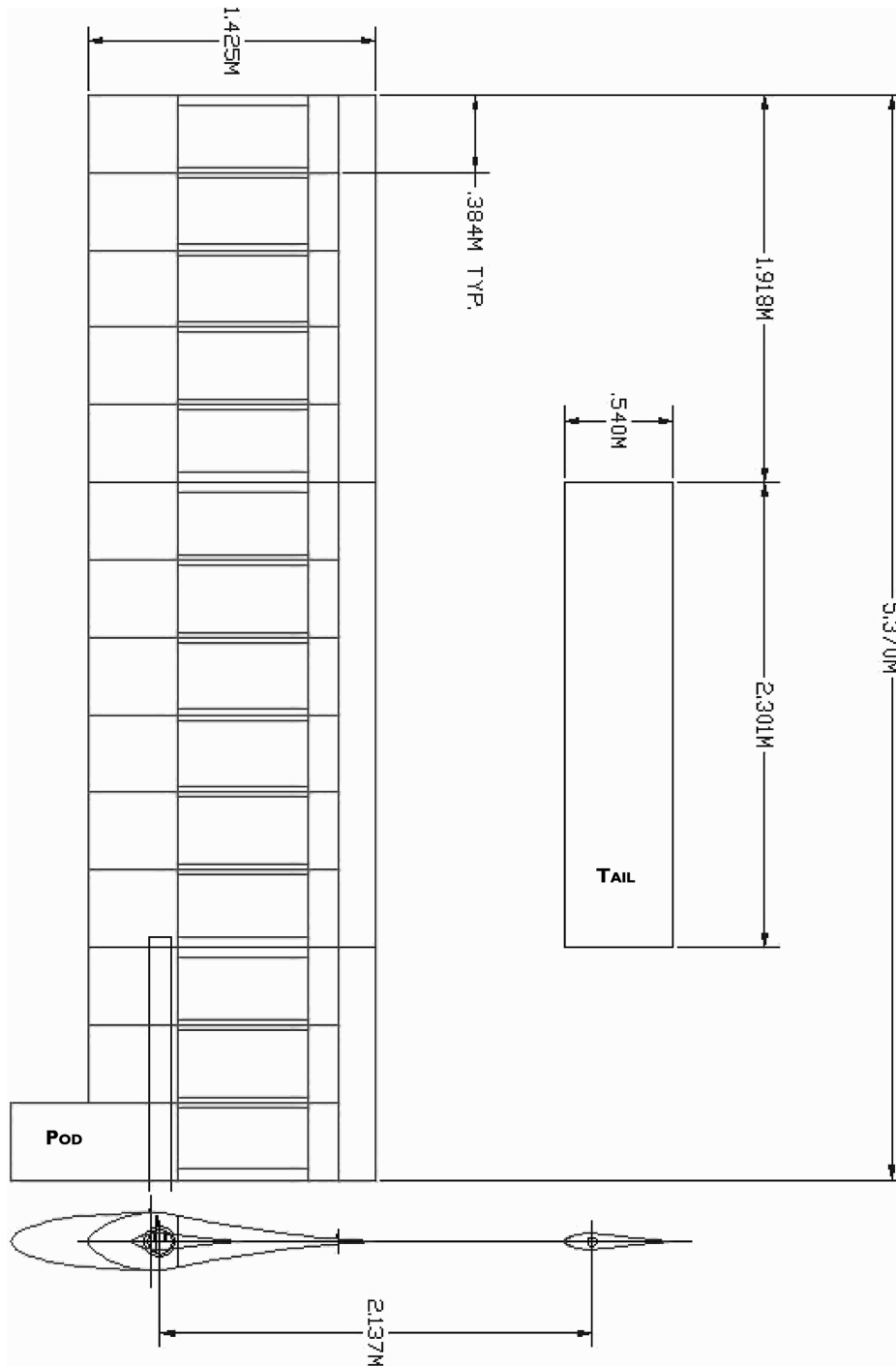


Fig. 5 Engineering layout of the wingsail.

The second main advantage of a wingsail for propulsion is the small actuation effort required. Because a cloth sail is fixed to the mast and trimmed from the boom, the center of pressure is aft of the leading edge. Thus, the trim force must overcome a portion of the lift of the sail. Inspection of a conventional sailboat shows a large block and tackle and winches required to hold the boom and trim the main sail. To control this effectively in an automatic manner requires a very large and fast-acting actuator. These types of actuators are typically expensive and would be prohibitive both in cost and power. By contrast, the wing is designed to pivot near the center of pressure of the wing itself and can be trimmed either directly or through an auxiliary trimming surface (tail). In either case, a small dc motor can actuate the wing.

The third main advantage of the wingsail over the conventional sail is the ability to make the wingsail self-trimming. That is, the wing

will fly at a constant angle of attack α to the relative wind. The benefit of this is that the wing will absorb gusts and decouple the propulsion system from the guidance system through passive stability (self-trimming), which greatly simplifies control system design. Through proper arrangement of the flying surfaces, the wingsail will readjust automatically to a change in wind direction with no intervention from pilot or control system.

The self-trimming capability makes the wingsail ideal for an autonomous sailboat because it reduced the disturbances from wind propulsion and eliminates the requirement for a very large and fast-acting actuator to constantly retrim the sails. Direct intervention is required only when the true wind crosses the longitudinal centerline of the boat, when the flap and tail are reversed from their previous positions. Note that, in a conventional sense, this corresponds to tacking (when the wind is from the front) and jibing (when the wind is

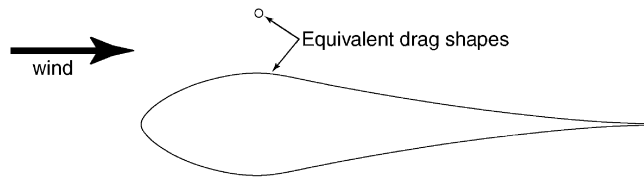


Fig. 6 Demonstration of the equivalent drag sections at Reynolds number of 229,000.

from the stern). Note that jibing and tacking the wingsail are very gentle and controlled because the bearings allow the sail to rotate 360 deg about the mast without interference, and thus the wing can point straight into the wind with no ill effects.

Conventional sails have one serious advantage: due to their sharp leading edge, they tend to be insensitive to Reynolds number variation. This alone may explain why they have persisted on modern designs even after the preponderance of evidence has demonstrated that wings are superior. Also, for sails below a certain size, a rigid wing will almost certainly be heavier due to the square-cubed law, with respect to the strength of structures and external stays from the top of the mast. Above a mast height of approximately 20 m, however, the structure of the mast could just as easily be incorporated into the spar of a wing. In [10], a race between two similar catamarans with a rigid wing and a conventional sail was analyzed. The winged catamaran had superior aerodynamic performance on all points of sail, but increased weight resulted in greater drag on the hulls due to the extra displacement. All legs that were raced at wind speeds greater than 8 kt were won by the winged catamaran, but all legs below 8 kt were won by the conventionally sailed catamaran.

III. Reynolds Number Effects

As mentioned previously, the Reynolds number effects of the wingsail section design must be accounted for to maximize the performance of the wing. Ignoring these Reynolds number effects has been the largest failing of wingsails to date, resulting in sections with poor performance in the field and, in turn, delaying the transition to rigid wings on sailboats.

Several low Reynolds number effects make design of high-lift sections difficult and are discussed at length in [11]. Typically, the flow about an airfoil at low Reynolds numbers is almost entirely laminar and cannot withstand either sharp radii or severe adverse pressure gradients without separation (and consequential very large drag rise). Often the flow separates, but then reattaches, causing a laminar separation bubble whose flow eddy results in a very large increase in the base drag of the section, and as soon as the section is put at an increased angle of attack, the laminar separation bubble bursts, causing large-scale flow separation, effectively limiting the maximum lift coefficient attainable.

In [12], the designers demonstrate a knowledge of the difficulties in designing good sections at these Reynolds numbers, but fail to capitalize on this knowledge and find an appropriate design. They correctly identify the proper Reynolds number range for sail operation as 200,000–1.2 million, and complain that “good low Reynolds number aerodynamic data applicable to sails are not readily available.” At that time, however, low Reynolds number computer codes had not yet reached maturity. Although correctly identifying the problem, they did not have the tools to find the ideal solution.

The reason that low Reynolds number airfoil sections do not exist for this range (which corresponds to small glider models) has to do with the unique requirements and subtle differences of sailing vehicles. Both the model glider and the sailboat require a high lift/drag L/D ratio. In a glider, this corresponds to glide distance or a minimum sink condition. In a sailboat, this corresponds to the ability to point upwind. Second, both a model glider and a sailboat require a high maximum C_L . In the case of the glider, this corresponds to slow flight while circling tightly in thermals; in a sailboat, the configuration is maximum speed while sailing across or downwind.

A sailboat wing, however, must be symmetrical to sail equally to both port and starboard.

IV. Symmetry

An airfoil section can be designed to be either symmetrical or asymmetrical. An asymmetrical section can always achieve a higher maximum lift coefficient and a higher lift/drag ratio than a symmetric section. Symmetric sections have the advantage of identical lift characteristics with both positive and negative angles of attack. Symmetry arguments become important in sailing vessels because a sailboat is required to sail equally well to both port and starboard, thus the section must be symmetrical. The model glider is rarely required to fly inverted, and certainly not for long periods of time. Thus, model glider sections are always asymmetrical to maximize the L/D .

Certain sailboats, including the designs in [13],^{†‡} attempt to capture the maximum L/D by using an asymmetrical section, but then tack and jibe “over the top.” This means that the wing is pinned midway up its span, then flipped to a horizontal position, and finally the bottom and top ends are then switched as the tack or jibe is completed. Needless to say, this results in an extremely heavy structure at the pin joint, as well as an exposed support or mast, which greatly increases the overall drag on the superstructure of the boat. It also makes wing control during this maneuver difficult in strong winds.

Using modern airfoil design techniques and a simple plain flap, one can achieve very close to the maximum C_L of an asymmetrical section. Thus, the increased weight, complexity, drag, and loss of the ability to self-trim in an asymmetrical design seem hardly worth the effort. Indeed, the ease of handling a symmetric section which does not pivot horizontally about the mast allows an increase in wing area, thus making up for the lower maximum lift coefficient. Although some continue to advocate over-the-top designs, they seem to stem more from novelty than an true understanding of aerodynamic tradeoffs.

V. Airfoil Section Design

The design goal for the section is to achieve a maximum lift coefficient of 1.8 in a Reynolds number range of 200,000–250,000. This can be achieved using a simple plain flap of constant flap/chord ratio. The desired pitching moment coefficient is small with the flap deflected, so as to be easily balanced by the tail. Also, the greater the lift/drag ratio, the better the upwind performance.

To match the total force on the wing at a wind speed of 5 kt with a theoretical lift coefficient of 1.8, the resulting Reynolds number is 229,000. Figure 7 shows the wind velocity required to achieve this Reynolds number as a function of angle from the true wind, and varies from 3.8 to 6 kt. This calculation is based on the assumption that the sailboat can sail at one-third of the true wind speed.

The wing has one-third the area of the sails, but generates 3 times the lift at its design point. This was chosen to enable a comparison of performance between the wing and sail. Note that the performance improves as the Reynolds number increases, but that the difficulty is in the low Reynolds number regime.

To achieve the desired goals of maximum lift coefficient of 1.8, lift/drag ratio of better than 20, and optimization for a Reynolds number of 229,000, a rather unusual design emerges. The high-lift coefficients require a very thick section where the entire lift is generated on the forward section, typical of the Liebeck “rooftop” sections. The boundary layer requires a trip strip that will force the transition from laminar to turbulent, placed symmetrically on the top and bottom surfaces. Typically, these trip strips are a thick material with a zigzag leading edge that is affixed to the surface at the desired location. The zigzag causes a small-scale vortex to form which pulls in the higher energy flow outside of the boundary layer, and though

[†]Cornell University, Rigid Airfoil Team, <http://www.dcaonline.com/raft/index2.html>.

[‡]Quinton, B., Boatek website, <http://www.boatek.demon.co.uk>.

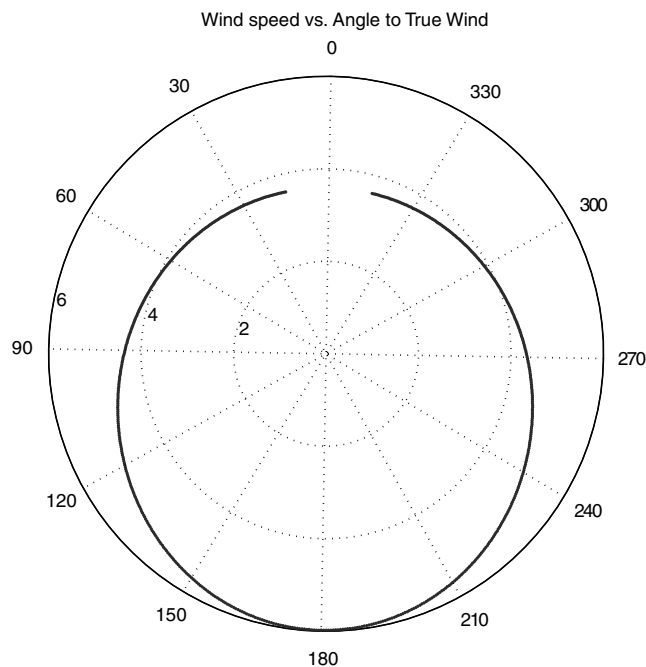


Fig. 7 Polar plot of the true wind speed vs the angle to the true wind for a Reynolds number of 229,000.

viscous drag increases, separation (and thus form drag) is delayed. Note that recent investigations in [14,15] suggest that the boundary-layer trips will not be as effective as XFOIL predicts. The boundary-layer transition forced by the strips occurs farther downstream than expected, and thus reduces their effect. Experimental validation will be required to validate the trip strip performance, and will necessitate careful measurements, as the presence or absence of laminar separation bubbles are not easily determined in the unsteady airflow near the surface of the water.

In addition to the short, flat pressure distribution on the section, the entire aft portion of the section is given to pressure recovery of the flow, preventing flow separation from the section surface. Thus, the back three-quarters of the section do not contribute at all to the lift, but merely ensure that the airflow can recover gracefully to freestream conditions.

A. Analysis Tools

To design the wing and tail sections, modern computational fluid dynamics (CFD) computer codes are used to predict performance and refine the design of the sections. The two main codes used for this are Ilan Kroo's PANDA and Mark Drela's XFOIL.

PANDA (Program for Analysis and Design of Airfoils) was developed by Professor Ilan Kroo in the 1980s at Stanford University.[§] The program computes and graphically displays the pressure distribution (in coefficient form) of airfoil sections in subsonic flow. PANDA calculates the inviscid pressure distribution over the airfoil at a specified angle of attack and Mach number; lift and pitching moment coefficients are also computed. The analysis is done with remarkable speed (less than a second), so that the effects of changes in angle of attack or airfoil geometry can be easily studied. Boundary-layer properties are computed based on this inviscid pressure distribution, and the location of transition, laminar or turbulent separation, and total drag are determined based on integral boundary-layer methods. It is possible to specify a position for "transition grit" or "trip strip" on the upper and lower surfaces to force transition or model surface roughness.

A major feature of the PANDA program is its provision for rapidly changing the airfoil geometry interactively. A smoothly faired bump (with specified but editable height and width) is added to the section,

and the new pressure distribution is quickly redrawn. In this way, the airfoil can be rapidly reshaped to produce a desirable coefficient of pressure C_p distribution.

XFOIL 1.0 is a CFD code that was written by Mark Drela in 1986 at the Massachusetts Institute of Technology [16,17].[¶] The main goal was to combine the speed and accuracy of high-order panel methods with the fully coupled viscous/inviscid interaction method used in the more sophisticated codes developed by Drela and Giles [18,19]. A fully interactive interface was employed from the beginning to make it much easier to use than the traditional batch-type CFD codes. Several inverse modes and a geometry manipulator were also incorporated early in XFOIL's development, making it a fairly general airfoil development system.

XFOIL is a much more full-fledged code than PANDA, able to operate well into the low Reynolds number regimes with excellent predictive capabilities. It also includes the ability to use either free or forced boundary-layer transitions and to predict lift and drag polars to just beyond the maximum lift coefficient.

B. Wing Section

Section development starts with a NACA 00xx section to probe the design space. The NACA section is then modified using PANDA until reasonable performance is achieved. At this point, the section coordinates are transferred to XFOIL which is used to iterate on the pressure distribution and boundary-layer trip-strip location until the results converge.

The first attempt used a NACA 0015 airfoil section. Although this airfoil section is known to have poor performance at low Reynolds numbers, it is the de facto standard for symmetrical sections and serves as a benchmark for comparison. Land yacht designers are using NACA 00xx sections almost exclusively in their successful designs. Part of their rationale behind their choice is the observation that the main drag source is not parasitic but rather induced drag. Because induced drag is largely a function of the aspect ratio \mathcal{AR} of the wing and the load carried by the wing, the effect of airfoil section is minimal. This gross analysis, however, fails to take into consideration the loading variation of the wing and the problems of stall and separation. Although the wing might be flying at a coefficient of lift below stall, sections of it might be above due to variations in wind speed with height (wind gradient) or effective twist. These problems can only be addressed with high maximum lift coefficient and the NACA 0015 simply cannot provide it. Figure 8 shows the poor performance of the NACA 0015 at low Reynolds numbers, where the flow is largely laminar. Note the laminar separation bubble (LS) on the top surface, the turbulent separation (TS) indicating trailing-edge stall, and the rather low L/D ratio.

The laminar separation bubble, indicated by the LS in Fig. 8, can be seen more clearly in Fig. 9, where the effect of the laminar separation bubble causes boundary-layer growth and subsequent contraction as the flow reattaches following the laminar separation. The laminar separation bubble affects the entire flow of the section, from the $C_{L_{max}}$ attainable to the manner in which the section stalls. The stall is likely to occur at the point of the bubble rather than at the trailing edge, resulting in a sudden loss of lift and increase in drag, which affects how close to $C_{L_{max}}$ one can sail.

The final design, after many iterations, results in a rather unusual shape. First, the final wing section is enormously thick, with a thickness-to-chord ratio of over 21%. The distribution of that thickness is predominately toward the nose of the section, consistent with the requirement that most of the lift be generated at the front part of the section before the trip strip, whereas the entire aft section is there only for pressure recovery.

Close inspection of Fig. 10 shows that the post-boundary-trip curvature is in fact concave, making construction using a normal cloth covering a challenge. As the cloth covering shrinks, it will tend to pull off of the curved rear section of the airfoil because a straight line connecting the point of maximum cross section and the end just

[§]Kroo, I., PANDA website, <http://www.desktopaero.com/PANDACatalogPage.html>.

[¶]Drela, M., XFOIL website, available online at: <http://raphael.mit.edu/xfoil>

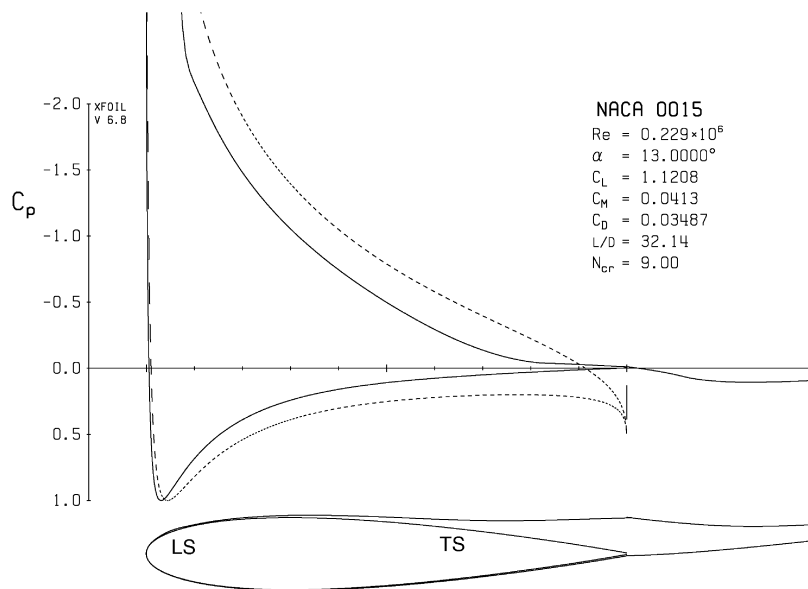


Fig. 8 XFOIL results for NACA 0015 airfoil at Reynolds number of 229,000 and C_L of 1.12.



Fig. 9 Close-up view of the laminar separation bubble on NACA 0015 airfoil at Reynolds number of 229,000.

before the flap hinge is shorter than the actual surface. The pressure distribution demonstrates the design challenges that were presented and how they were solved. Note the absence of either laminar separation bubbles or turbulent separation at the end of the section (with a C_L of 1.04, with no flap deployment).

The salient features of the pressure distribution is the flat top, corresponding to a uniform suction on the upper front surface. The pressure begins its recovery just after the trip strip located at the 22% chord point and very smoothly recovers back to freestream pressure

without separation. Note that the flow is actually accelerating on the lower surface below the stagnation point. This causes the upward slope of the lower line in the pressure distribution, indicating some suction existing at the maximum thickness point of the final wing section. Aft of the maximum thickness lies a very smooth pressure recovery all the way to the rear point of the airfoil section. Reemphasizing, there are no laminar separation bubbles and no turbulent separation. Again, we note that recent efforts have demonstrated that the trip strips may not work as well in practice as predicted.

The airfoil section is not close to stall but will stall gently from the rear, progressing forward, resulting in a very gradual loss of lift and increase in drag as the angle of attack is increased. This is important due to the varying nature of the wind (demonstrated in Fig. 2 in the lower graph). A conventional section like the 0015 will often abruptly stall and lose lift, resulting in poor perceived sailing performance. The tail is designed in exactly the same manner, except for a lower Re of 44,000 and without a flap (see Fig. 11).

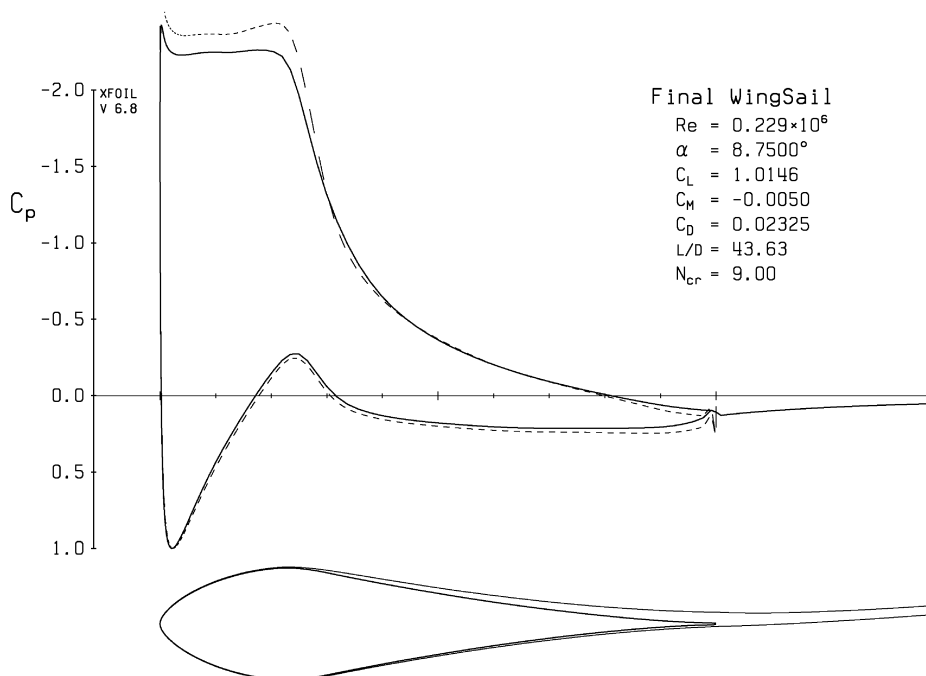


Fig. 10 Final wingsail airfoil section and pressure distribution, Reynolds number of 229,000, and a lift coefficient of 1.0.

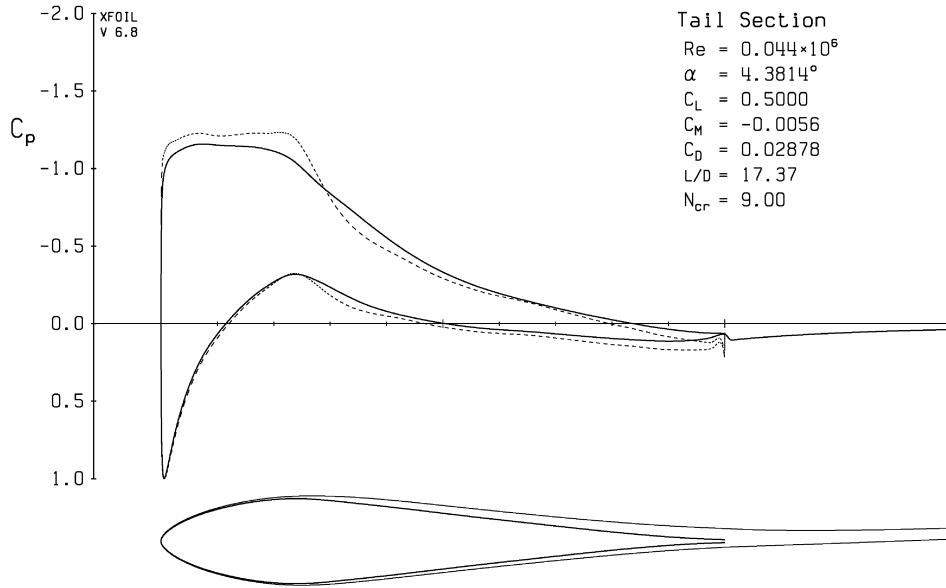


Fig. 11 Pressure distribution of the final tail section at a Reynolds number of 44,000 and a lift coefficient of 0.5.

C. Flap/Chord Ratio

To increase the coefficient of lift of the main wing section and obviate the need for over-the-top tacking and jibing, a simple plain flap is used to effectively increase the chamber of the wing. Figure 12 shows the pressure distribution with the flap deflected 45 deg. Note that the flow separates off the back of the flap, causing an increase in drag. Unfortunately, at these low Reynolds numbers, the flow cannot negotiate the curvature of the flap hinge, regardless of where it is placed on the airfoil section, meaning that the flow will separate as soon as the flap is deflected more than a few degrees. Thus, the design trades the separated flow and subsequent drag for increased lift. Low Reynolds number flow pushes the design toward a very small flap/chord ratio and large deflection. In other words, a small trailing-edge tab deflected a great deal will turn the flow enough to give effective

chamber, while giving the flow only the smallest area from which to separate.

A grid point search of the flap/chord ratio c_f/c is performed using XFOIL to find the minimum drag at a C_L of 1.8. The flap/chord ratio is varied from 1 to 40% in 1% increments (see Fig. 13). Both the maximum attainable lift coefficient as well as the lift to drag ratio at that lift coefficient are plotted, and both reach their maximum near $c_f/c = 13\%$.

The final main wing section is shown in Fig. 12, with the flap deflected 45 deg. The aggregate plots of the lift-to-drag coefficients for the final section with the flap deployed can be found in Fig. 14. The plot shows that there exists an “efficient boundary” where the lift/drag ratio is maximized for a given lift distribution. This will then become the basis of aerodynamic control: once the desired lift

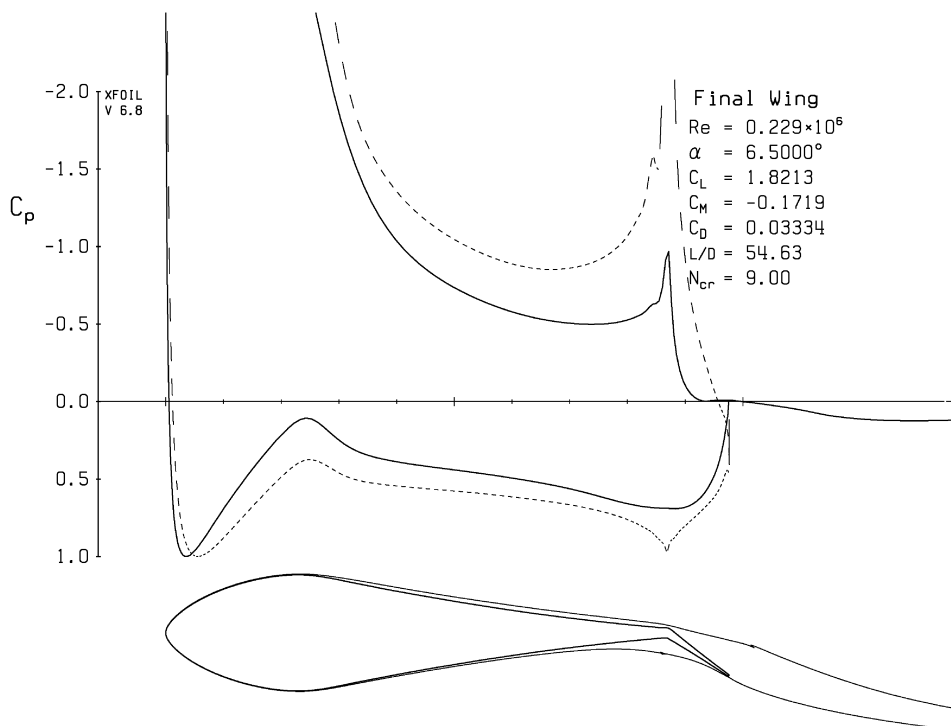


Fig. 12 Pressure distribution of main wingsail section with flap deployed, Re of 229,000 and a C_L of 1.8.

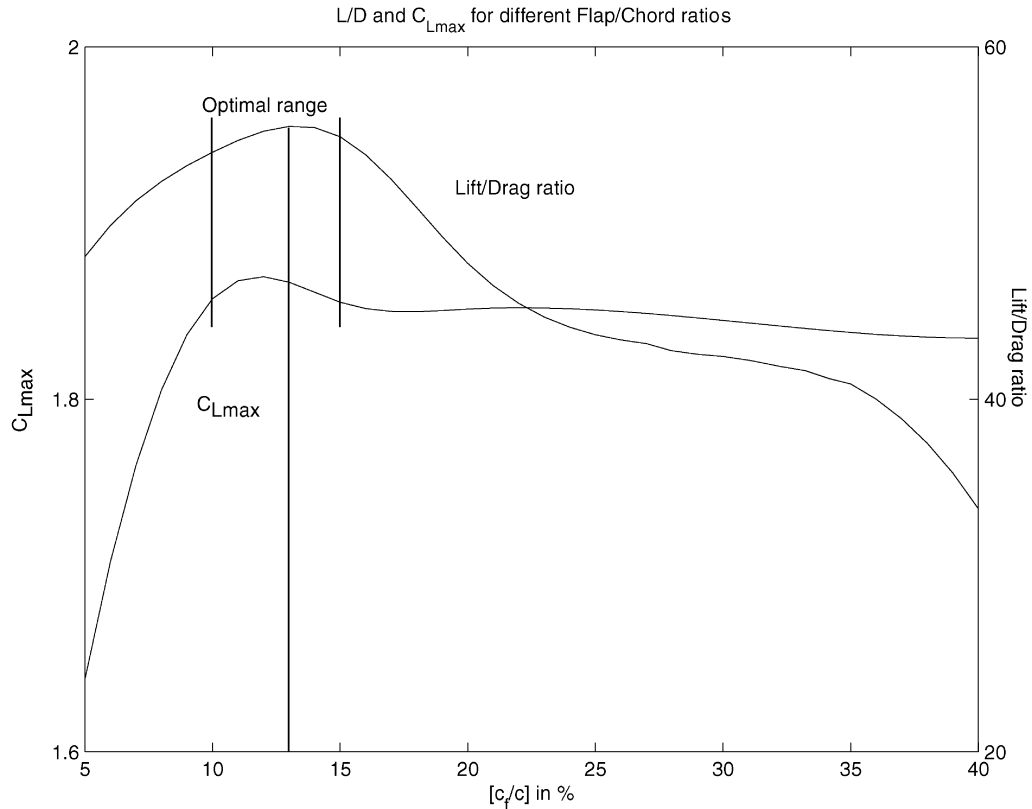


Fig. 13 Results of the grid point search for optimum flap performance.

coefficient is determined, the correct flap setting can be chosen to minimize the drag.

Note that, above a C_L of 1.8, the drag continues to increase without any further increase in lift. This is expected from the increase in separation of the flow, and as predicted is gradual. Looking at the data

in a different way, it is useful to visualize the lift/drag ratio as a function of either lift, drag, or angle of attack (as in Fig. 15). Note also that the angles of attack involved are uniformly small, implying that the control over the tail must be precise or the wingsail will repeatedly stall while underway.

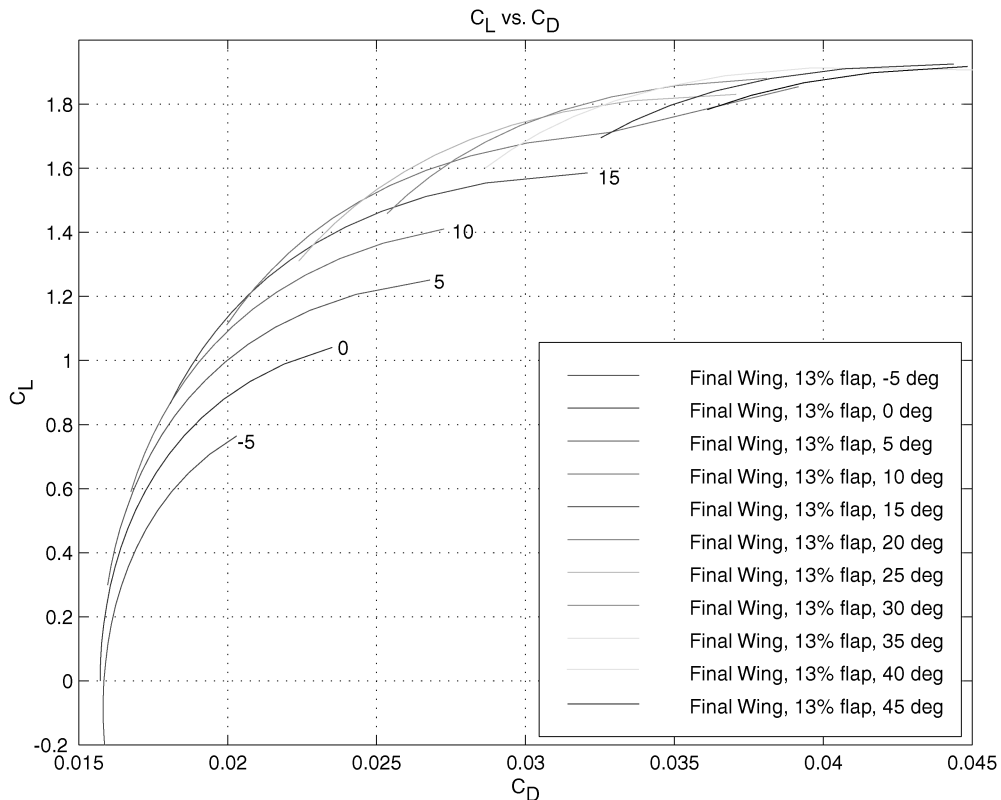


Fig. 14 Coefficients of lift vs drag for the final wing section with flap deployed at Re of 229,000.

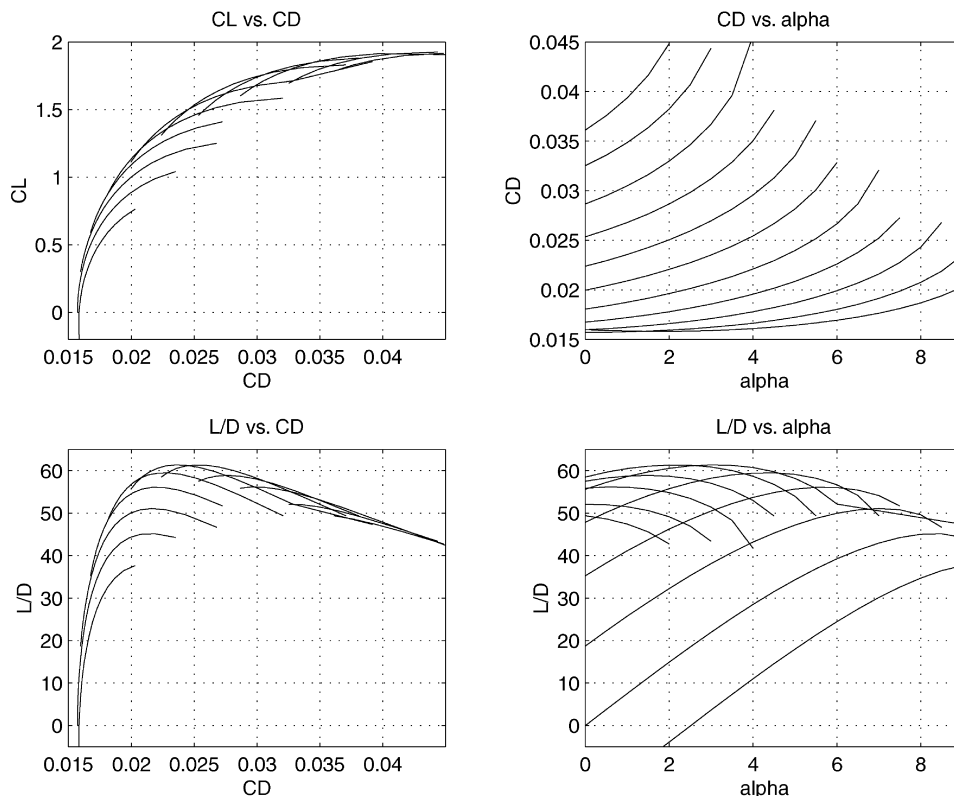


Fig. 15 Aerodynamic polars for the main wingsail with flap deployed at Re of 229,000.

VI. Wing/Tail Configuration Analysis

Two possibilities exist for actuating the wing and controlling its angle of attack. The first possibility is to control the angle of attack mechanically using an actuator that rotates the wing about the mast. This has the advantage of quick actuation, and correct placement of the rotation axis can keep the forces low. However, the variability of the wind will require high-frequency actuation and closed-loop control to keep the wing correctly trimmed. Furthermore, the entire range of angles of attack between zero lift and stall is less than 12 deg, which translates into a closed-loop tracking requirement that is challenging to meet.

The other possibility for angle-of-attack control is to use an auxiliary surface to trim the wing aerodynamically; this can take the form of a tail behind the wing (conventional), a trimming surface in front of the wing (canard), or attached to the trailing edge of the wing (flying wing). There are also trisurface configurations, but these were considered too complex for implementation. The actuator in this case moves the trimming surface only. By designing the auxiliary surface such that the wing/surface assembly is passively stable with respect to angle of attack, the entire system will track the relative wind automatically. This is advantageous over active control in terms of actuation effort, simplicity of design, and overall performance.

With the main wing section and tail section designed, various arrangements of wing and tail can now be considered. The main criteria for consideration is angle-of-attack stability with respect to change in wind direction or velocity. The configuration must be able to trim a C_L of 1.8 with a flap deflection of 45 deg (with the increased pitching moment due to the flap about the pivot point). Formally, these requirements can be written as

$$C_m = 0 \quad (1)$$

$$\frac{\partial C_m}{\partial \alpha} < 0 \quad (2)$$

The system is in trim (pitching moment of the entire wing/tail system about the pivot point should be zero), and the wing/tail

system should be stable with respect to angle of attack (the change in pitching moment with a change in angle of attack should be negative). A perturbation of the angle of attack in a positive sense will cause a negative (or nose down) pitching moment, which will reduce the angle of attack, and likewise a negative angle-of-attack perturbation will cause an increase in the pitching moment (nose up) and will increase the angle of attack. Note that the reference to up and down is simply a convention to relate the wing terminology back into the intuitive reference of flight [20,21]. In fact, there is no up or down, rather port or starboard, and the important feature missing from these equations are the gravity terms, which do not come into play in the boat aerodynamics.

The other considerations are mechanical complexity, control power, and a minimum swept radius of the farthest point away from the mast. The minimum swept radius constraint is due to the fact that, to remove the coupling between angle of attack of the wingsail and heeling angles, the wing/tail assembly must be mass balanced about the mast so that pitch and roll of the hull does not induce changes in angle of attack (a tail heavy wing/tail assembly would result in an increase in angle of attack with roll angle, thus inducing instability in close hauled conditions).

Fekete and Newmann [22] performed a simplified analysis of the conventional and canard configurations. In this paper, that analysis is refined by using higher fidelity models for downwash and induced drag as well as correcting for finite aspect ratio effects. Furthermore, two other configurations, the “flying wing” and the “free-floating canard,” are analyzed using the same tools.

A. Methodology

To keep the problem tractable, a combination of thin airfoil theory and simplified lifting line theory, as discussed in Glauert [23], is used for the entire analysis. This provides a simple yet accurate and consistent method of accounting for flap deflection (thin airfoil theory) and three-dimensional flow effects (lifting line theory) in the form of an aspect ratio correction. Lifting line theory assumes that the airfoil is flat and imposes a bound vortex to induce circulation and create the corresponding (inviscid) lift. The drag terms ignore any

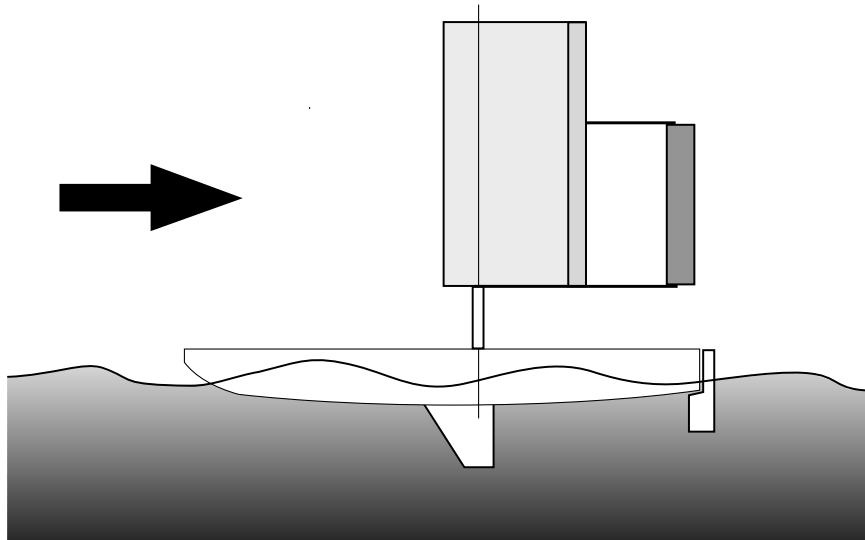


Fig. 16 Conventional configuration with the tail behind the wing.

parasitic effects. In the specific case of this configuration analysis, first consider the main wing with flap deployed.

Define the flap effective angle, and using the previously selected c_f/c ,

$$\Theta_f \equiv \arccos\left(2\left[\frac{c_f}{c}\right] - 1\right) = 0.2402 \quad (3)$$

$$\alpha_\delta \equiv 1 - \frac{\Theta_f - \sin(\Theta_f)}{\pi} = -0.449 \quad (4)$$

where α_δ is the flap lift coefficient conversion factor used in

$$C_L = C_{L_\alpha}[\alpha + \alpha_\delta \delta_f] \quad (5)$$

where α is the airfoil angle of attack and δ_f is the flap deflection. However, from lifting line theory, the 3-D correction for the 2-D lift coefficient (given from thin airfoil theory as 2π), and assuming an elliptical lift distribution, is

$$C_{L_\alpha} = \frac{2\pi AR}{AR + 2} \quad (6)$$

For the pitching moment about the quarter-chord point, we use

$$\mu_1 \equiv \frac{1}{2} \left(1 - \left[\frac{c_f}{c}\right]\right) \frac{\sin(\Theta_f)}{\pi - \Theta_f + \sin(\Theta_f)} = 0.2075 \quad (7)$$

which is used in defining the moment coefficient conversion factor

$$\mu_\delta = -\mu_1 \alpha_\delta \left[\frac{c_f}{c}\right] = -0.0121 \quad (8)$$

where the pitching moment coefficient C_M is due only to flap deflection:

$$C_M = \mu_\delta C_{L_\alpha} \delta_f \quad (9)$$

Using Eqs. (5–9), the aspect ratio of the wing, and the computed values give the basic relationships required to analyze the various configurations.

B. Conventional Layout

The conventional layout, pictured in Fig. 16, has the wing forward, followed by a tail some distance back. This has the immediate disadvantage of being tail heavy. This requires ballast forward to place the center of mass at the quarter-chord point of the main wing. In terms of a wing, ballast is useless weight. Because the weight must be attached to the wing, this further raises the center of gravity of the

boat, increasing the susceptibility to capsize. Additionally, the swept radius of the tail is quite far back. This means that in close quarters (such as berthing), the tail may swing out beyond the catamaran hulls and strike an adjacent vessel.

Figure 17 shows all of the force and moment vectors acting on the conventional wing and tail. To trim the wingsail, the moment about the pivot point must be zero [Eq. (1)], and to guarantee passive gust stability, the derivative of the moment equation with respect to the angle of attack must be negative [Eq. (2)]. Using Fig. 17 as a reference, we first expand the wing lift term:

$$L_W = \frac{1}{2} \rho V^2 S_W (C_{L_\alpha})_W (\alpha + \alpha_\delta \delta_f) \quad (10)$$

where L_W is the wing lift, ρ is the air density, V is the freestream relative wind velocity, S_W is the wing area, α is the angle of attack of the wing, and δ_f is the flap deflection. Likewise, the wing pitching moment term is

$$M_W = \frac{1}{2} \rho V^2 S_W c_W (C_{L_\alpha})_W \mu_\delta \delta_f \quad (11)$$

where M_W is the pitching moment about the quarter chord point (defined as positive [+] nose up), c_W is the wing chord length, and μ_δ is defined in Eq. (8). Finally, the tail lift is

$$L_T = \frac{1}{2} \rho V^2 S_T (C_{L_\alpha})_T \left(\alpha + \delta_T - \frac{\epsilon}{2}\right) \quad (12)$$

where L_T is the tail lift, S_T is the tail area, δ_T is the tail deflection relative to the main wing chord line, and $\epsilon/2$ is the downwash angle at the main wing. Note that ϵ is defined as the far-field (or Trefftz plane) downwash and, at the tail, it is half of the far-field value. For an

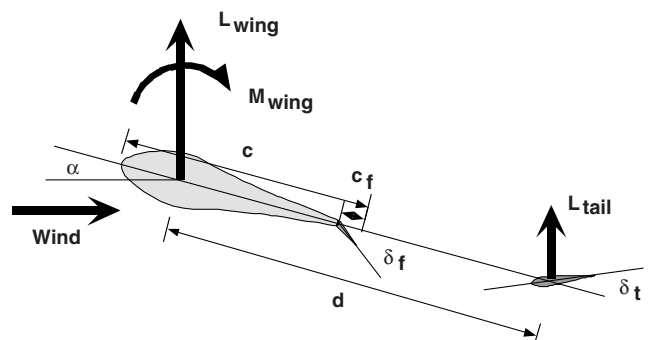


Fig. 17 Forces and moments on the conventional configuration.

elliptically loaded wing, the downwash at the tail is

$$\frac{\epsilon}{2} = \frac{C_L}{\pi AR} = \frac{2[\alpha + \alpha_\delta \delta_f]}{AR_w + 2} \quad (13)$$

Using Eqs. (10–12), we define the moment balance about the pivot point (located at the quarter chord) as

$$\sum M_\oplus = M_W - d \times L_T \quad (14)$$

where d is the moment arm from the pivot point to the quarter chord of the tail, and is measured positive [+] *aft*. Substituting in Eqs. (11) and (12)

$$M_\oplus = \frac{1}{2} \rho V^2 S_W c_W (C_{L_\alpha})_W \mu_\delta \delta_f - \frac{1}{2} \rho V^2 S_T d (C_{L_\alpha})_T \left(\alpha + \delta_T - \frac{\epsilon}{2} \right) \quad (15)$$

Dividing out the dynamic pressure and turning it into coefficient form, and substituting in

$$C_{M_\oplus} = \frac{M_\oplus}{\frac{1}{2} \rho V^2 S_W c_W} = (C_{L_\alpha})_W \mu_\delta \delta_f - \left(\frac{d}{c_W} \right) \left(\frac{S_T}{S_W} \right) (C_{L_\alpha})_T \left[\left[\frac{AR_w}{AR_w + 2} \right] \alpha + \delta_T - \frac{2\alpha_\delta \delta_f}{AR_w + 2} \right] \quad (16)$$

Define a nondimensional length and area ratio

$$\bar{d} \equiv \frac{d}{c_W} \quad (17)$$

$$\bar{S} \equiv \frac{S_T}{S_W} \quad (18)$$

Substituting the preceding definitions and rearranging Eq. (16)

$$C_{M_\oplus} = \left[(C_{L_\alpha})_W \mu_\delta - \bar{d} \bar{S} (C_{L_\alpha})_T \frac{2\alpha_\delta}{AR_w + 2} \right] \delta_f - \bar{d} \bar{S} (C_{L_\alpha})_T \left[\frac{AR_w}{AR_w + 2} \alpha + \delta_T \right] \quad (19)$$

Inserting Eq. (6) using both the wing and the tail ARs, and evaluating the stability criteria [Eq. (2)], notice that only the last term in Eq. (19) depends on α , thus

$$\frac{\partial C_{M_\oplus}}{\partial \alpha} = -\bar{d} \bar{S} (C_{L_\alpha})_T \left[\frac{AR_w}{AR_w + 2} \right] \quad (20)$$

Given that all the terms are positive, the stability criteria is met for all $d > 0$ (i.e., the tail must be behind the main wing). Using the results from XFOIL presented in Sec. V, the trim condition is evaluated with a $C_{L_{\max}}$ of 1.8 for the main wing with the flap deflected 45 deg, and a $C_{L_{\max}}$ of 0.75 for the tail. This results in a minimum trim condition, such that the tail is at its maximum lift coefficient at the same instant that the wing reaches its maximum lift coefficient. The minimum trim condition is realized for a “tail volume coefficient” of

$$\bar{d} \bar{S} > 0.00528 \pi^2 \quad (21)$$

Thus, in the case of the conventional wing/tail arrangement, both the stability criteria and the trim condition can be met, as long as the tail volume coefficient satisfies Eq. (21). The swept radius of the conventional configuration is the distance from the quarter chord to the end of the tail, which turns out to be

$$R_s = c_W \left[\bar{d} + \frac{3}{4} \bar{c} \right] \quad (22)$$

where \bar{c} is the ratio of the tail chord to the wing chord (c_T/c_W).

C. Canard

An alternate configuration is the “canard,” where the trimming surface is placed in front of the wing as pictured in Fig. 18. A canard aircraft has trim and stall problems that must be dealt with and can usually be designed for either passive stability or efficiency (i.e., reduced induced drag), but not both.

The overwhelming advantage a canard has for the sailboat propulsion system is that it is more easily balanced about its neutral point, making the entire setup lighter. Also, depending on the distances that occur for trim and stability, it is possible that the radius swept by the canard arrangement can be made small. Figure 19 shows the vectors and key distances on the canard configuration. Once again, it is required that the moment balance be zero [Eq. (1), trim] and that the change in moment be negative [Eq. (2), stability].

The wing lift and moment are the same as for the conventional configuration [Eqs. (10) and (11), respectively], however, the canard lift L_c differs from the tail:

$$L_c = \frac{1}{2} \rho V^2 S_c (C_{L_\alpha})_c (\alpha + \delta_c) \quad (23)$$

where S_c is the area of the canard, and δ_c is the canard angle relative to the canard/wing chord line. Again, with the distances d and sm

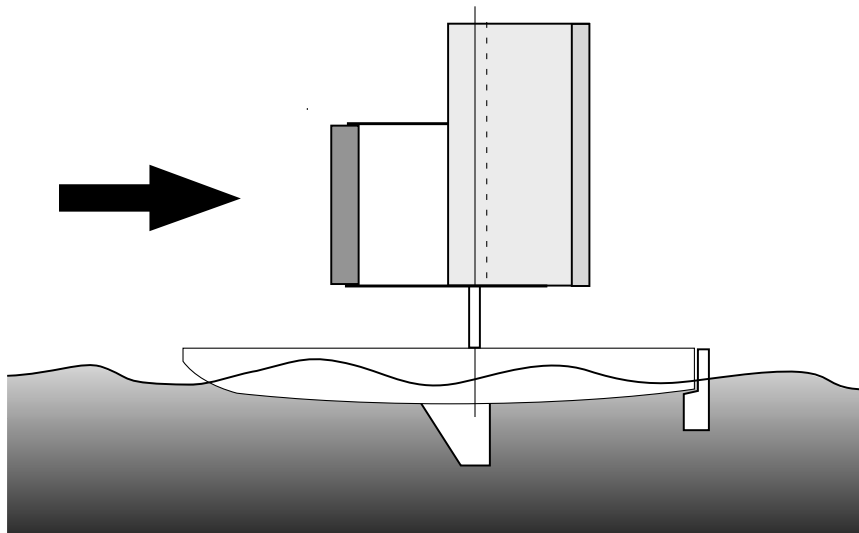


Fig. 18 Canard configuration, tail ahead of the main wing.

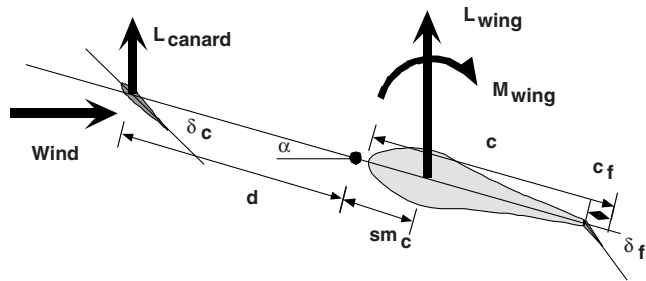


Fig. 19 Forces and moments on the canard configuration. Distances d and sm are measured positive aft of the pivot point.

defined as positive aft (see Fig. 19), the moment about the pivot point is

$$\sum M_{\oplus} = M_w - d \times L_c - sm \times L_w \quad (24)$$

which can be expanded, normalized, and grouped as

$$C_{M_{\oplus}} = (C_{L_{\alpha}})_w [\mu_{\delta} + \overline{sm} \alpha_{\delta}] \delta_f - \{ \overline{sm} (C_{L_{\alpha}})_w + \bar{d} \bar{S} (C_{L_{\alpha}})_c \} \alpha - \bar{d} \bar{S} (C_{L_{\alpha}})_c \delta_c \quad (25)$$

where the definitions are the same as Eqs. (17) and (18), with the addition of

$$\overline{sm} \equiv \frac{sm}{c_w} \quad (26)$$

Differentiating Eq. (25) with respect to α , the stability criteria is

$$\frac{\partial C_{M_{\oplus}}}{\partial \alpha} = -\{ \overline{sm} (C_{L_{\alpha}})_w + \bar{d} \bar{S} (C_{L_{\alpha}})_c \} < 0 \quad (27)$$

Again, both \overline{sm} and \bar{d} are defined as positive aft of the pivot point; \bar{d} in Eq. (27) is negative, whereas \overline{sm} is positive and \bar{S} is much less than one. The correction for the canard downwash is not as straightforward as for the conventional [Eq. (13)]. The downwash is calculated from biplane theory developed in the 1920s. Using Munk's stagger theorem [24], the downwash of the canard on the wing has roughly the same effect as the wing would have on the canard if the flow were reversed. Thus, the canard downwash correction modifies the lift curve slope of the main wing:

$$(C_{L_{\alpha}})_c = 2\pi \frac{\mathcal{AR}_c}{\mathcal{AR}_w + 2} \quad (28)$$

$$(C_{L_{\alpha}})_w = 2\pi \frac{\mathcal{AR}_w}{\mathcal{AR}_w + 2} \left(1 - \frac{2(C_{L_{\alpha}})_c \bar{S}}{\pi \mathcal{AR}_w} \right) \quad (29)$$

The canard trim condition and stability are related. For a given coefficient of lift and angle of flap deflection, the canard can be determined to both trim and be passively stable. Equations (25) and (27) are solved simultaneously to yield the required static margin \overline{sm} and canard volume $\bar{d} \bar{S}$.

This solution, however, is not robust; \overline{sm} and $\bar{d} \bar{S}$ are unique for only one specific flap deflection δ_f . For instance, if the trim and stability criteria are solved for a flap deflection of 45 deg and a C_L of 1.8, then, when the flap is deflected less than 45 deg, the canard configuration is not stable and will attempt to swap ends. If the trim and stability criteria are solved for zero flap deflection, then, at a high-lift coefficient, the canard will not generate sufficient lift to be able to trim the main wing with the flap deflected. The canard itself will stall before the main wing achieves high C_L .

Unfortunately, when using the canard configuration, one must choose to be stable or to have a high maximum lift coefficient, but not both. The canard configuration is not acceptable for this project. This is similar to the problem that canard aircraft have: very few of them have flaps on the main wing for decreased landing speeds. Those few that do have flaps on their main wings resolve this with exotic solutions, such as a variable sweep canard that changes the longitudinal center of the canard as the flaps are deployed (for an excellent treatment of the subtleties of canard designs, see [14,15]).

D. Flying Wing

If the desire is to minimize the swept radius of the wing, then certainly the flying wing would represent the optimal approach. Flying wings, however, almost always rely on washout of the tips to provide passive stability; the tips of the rearward swept wings are twisted nose down and act somewhat like a conventional tail. However, to make a symmetrical flying wingsail requires both trim and stability without any wing twist whatsoever, which is a difficult challenge.

One of the main differences of the flying wing from other configurations is that the wing can be tapered, rather than rectangular (see Fig. 20). The lift and moment equations are formulated for an infinitesimal slice of the wing shown in Fig. 21. The tip-to-root chord ratio is defined as λ , the sweep of the quarter-chord line as Λ_s , and the normalized span variable $\bar{y} \equiv y/b$, where y is the distance from the base of the wing to the tip, b is the semispan, and thus $dy = b d\bar{y}$. The wing chord as a function of \bar{y} is

$$c(\bar{y}) = \frac{2\bar{c}}{\lambda + 1} [(\lambda - 1)\bar{y} + 1] \quad (30)$$

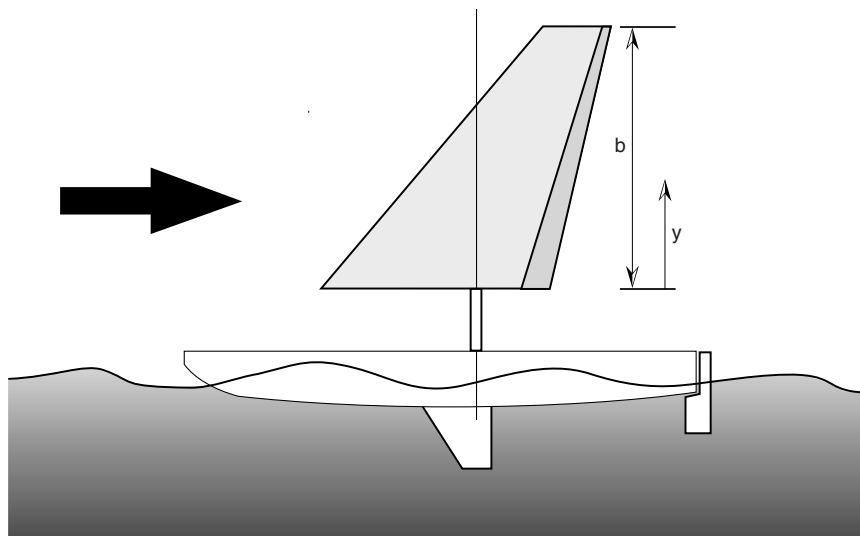


Fig. 20 Flying wing configuration for wingsail propulsion.

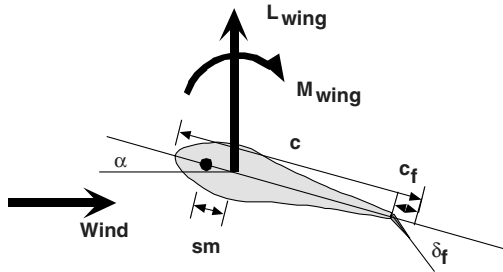


Fig. 21 Lift and moment vectors for the flying wing configuration.

where \bar{c} is the mean chord. Likewise, the location of the quarter-chord point of the wing with respect to the pivot point x_{qc} is:

$$x_{qc}(\bar{y}) = AR\bar{c} \tan \Lambda_s \bar{y} + sm_0 \tag{31}$$

where sm_0 is the offset from the root quarter-chord point to the pivot point and is analogous to the sm in the canard equations. With these basic geometric relationships defined, the lift and moment balance on the flying wing for a thin slice are calculated from

$$L_w = \int_0^1 l_w d\bar{y}$$

and

$$M_w = \int_0^1 m_w d\bar{y}$$

Integrating and evaluating the limits, the resulting moment balance is

$$C_{M_{\oplus}} = \frac{M_{\oplus}}{\frac{1}{2} \rho V^2 S_w \bar{c}} = C_{L_w} \left\{ \left[\frac{4\lambda^2 + \lambda + 1}{3(\lambda + 1)^2} \right] \mu_{\delta} \delta_f - \frac{1}{3} \left[AR \frac{2\lambda + 1}{\lambda + 1} \tan \Lambda_s + 3\bar{sm} \right] (\alpha + \alpha_{\delta} \delta_f) \right\} \tag{32}$$

where \bar{sm} is the offset normalized by the mean chord sm/\bar{c} . Note that only the second term is a function of α :

$$\frac{\partial C_{M_{\oplus}}}{\partial \alpha} = - \left\{ AR \frac{2\lambda + 1}{3(\lambda + 1)} \tan \Lambda_s + \bar{sm} \right\} < 0 \tag{33}$$

The stability bound is a fixed relationship between \bar{sm} and λ for any given Λ_s . Figure 22 shows the stability bound for a Λ_s range and demonstrates that, for a given λ , a minimum \bar{sm} cannot be exceeded or else the configuration is unstable.

Equation (33) indicates that, as long as the sweep angle is positive, and the offset from the mean aerodynamic quarter-chord point is less than the first term of Eq. (33), stability is ensured. The problem occurs when trimming the wing. Because of stability considerations, the second term in Eq. (32) is negative, thus the first term must be positive to trim the wing. The taper ratio λ can vary only from 0 to 1, however, and thus the term $\frac{4}{3}[(\lambda^2 + \lambda + 1)/(\lambda + 1)^2]$ will always be positive. For the flying wing to have a net zero moment on the wing, the quantity $\mu_{\delta} \delta_f$ must be positive, but from Eq. (8), μ_{δ} is negative. Thus, δ_f must be negative for trim; that is, the trailing-edge flap must be reflexed.

The only way for the flying wing to be both passively stable and have zero net moment is for the flap angle to be negative (or reflexed). Because the high-lift coefficient depends on a positive displacement of the flap, the maximum lift coefficient that can be achieved with the flying wing configuration (and reflexed flap) is approximately 0.8 based on XFOIL results. This performance is actually worse than the cloth sail, negating the advantages of a rigid wing.

The only way a flying wing aircraft can be both stable and trimmed is to reflex the trailing edge of at least a portion of the wing. An alternate solution in the case of the wingsail is to use a multisegment flap and trim part of the flaps in one direction and part in the other. By definition, however, this still means dumping lift and not being able to trim as high a C_L as the other viable solutions.

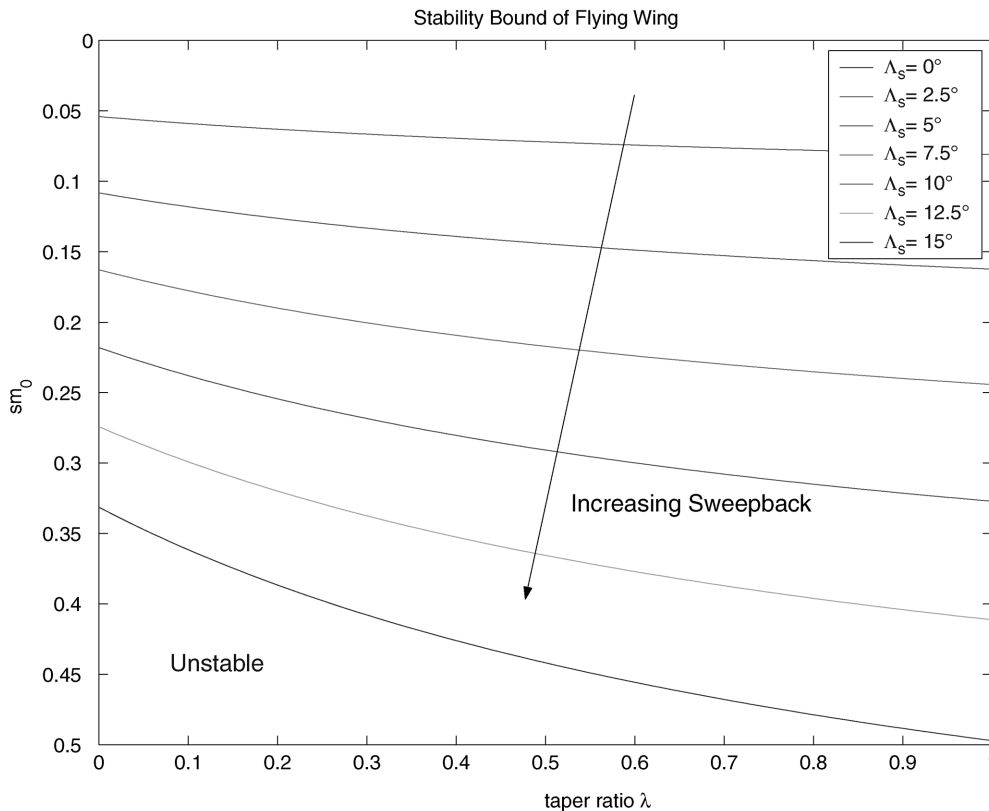


Fig. 22 Stability bound plot for flying wing configuration with a quarter-chord sweep angle Λ_s , taper ratio λ , and mast pivot offset point sm_0 .

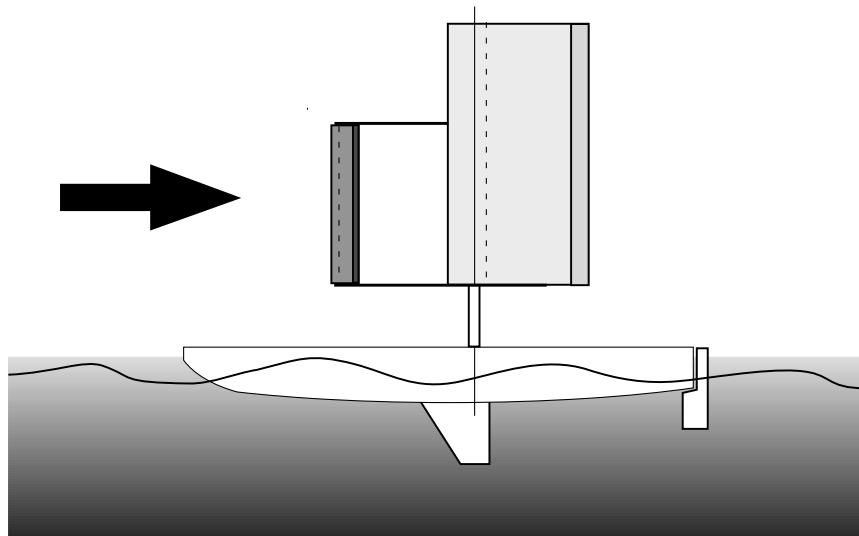


Fig. 23 Free-floating canard configuration.

E. Free-Floating Canard

The last configuration to be analyzed is the free-floating canard configuration, pictured in Fig. 23. The free-floating canard is an unusual configuration that was first used on the 1942 Curtiss XP55 Ascender without a great deal of success; the Ascender suffered from a divergent stall that led test pilots to mispronounce the aircraft’s name in a pejorative sense (describing the attitude in which it flew once stalled). Note that these problems were eventually solved, but the project never went into production.

What makes this configuration unique is that the canard itself is allowed to freely pivot in pitch and is trimmed via a trailing-edge flap. Thus, a change in wind direction or a gust causes the canard to rotate into a new trim position, which then, in turn, rotates the wing to its new equilibrium position. The key is that the canard itself is passively stable, and that the entire system retains stability. Forces and moments are detailed in Fig. 24.

The free-floating canard itself must be analyzed separately, and the requirements for the free-floating canard alone are identical to that of the entire system: the free-floating canard must be trimmed [Eq. (1)] and stable [Eq. (2)]. Figure 25 shows the free-floating canard with its own angle of attack, as well as its own trailing-edge flap. The free-floating canard is the same flying wing arrangement analyzed previously, with $\lambda = 1$ and $\Lambda_s = 0$. The conclusion that the flying wing configuration could not be stable and trim a high C_L remains and is indeed true of the free-floating canard. Based on XFOIL results, the reflexed trailing edge causes the canard to lose 33% of its lifting ability at a Reynolds number of 44,000. Thus, the $C_{L_{max}}$ that the free-floating canard can produce is 0.5, which is much lower than the equivalent conventional tail or canard airfoil.

The moment balance of the free-floating canard results in a fixed relationship between α_{free} and $\delta_{f_{free}}$:

$$\alpha_{free} = \left[\frac{\mu_\delta}{\overline{sm}_{free}} - \alpha_\delta \right] \delta_{f_{free}} \tag{34}$$

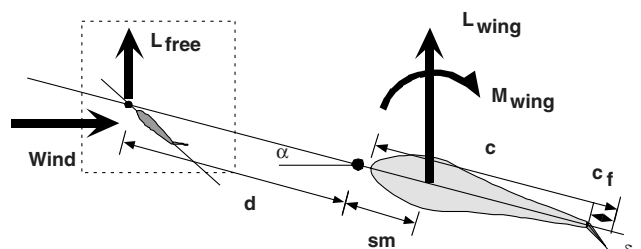


Fig. 24 Forces and moments on the free-floating canard configuration.

and a fixed expression for L_{free}

$$L_{free} = \frac{1}{2} \rho V^2 S_{free} (C_{L_\alpha})_{free} \frac{\mu_\delta}{\overline{sm}_{free}} \delta_{f_{free}} \tag{35}$$

The free-floating canard lift is purely a function of the canard flap angle δ_{f_c} . The remaining equations relating to the entire free-floating canard and wing system are analyzed for trim and stability. Referring to Fig. 24, the moment balance of the free-floating canard configuration is

$$C_{M_\oplus} = \frac{M_\oplus}{\frac{1}{2} \rho V^2 S_w c_w} = (C_{L_\alpha})_w [\mu_\delta + \overline{sm} \alpha_\delta] \delta_f - \{ \overline{sm} (C_{L_\alpha})_w \} \alpha - \overline{d} \overline{s} C_{L_{free}} \tag{36}$$

where the terms have all been previously defined and, again, both d and sm are negative forward. The stability criterion [Eq. (2)] is dependent entirely on the term $\overline{sm} (C_{L_\alpha})_w$ and is satisfied for all $\overline{sm} > 0$ (quarter chord of main wing aft of pivot point):

$$\frac{\partial C_{M_\oplus}}{\partial \alpha} = -\overline{sm} (C_{L_\alpha})_w^2 < 0 \tag{37}$$

The trim condition [Eq. (1)] requires the same corrections for the downwash of the free-floating canard that were used in the evaluation of the conventional canard configuration and are found in Eqs. (28) and (29).

Using the XFOIL result of a $C_{L_{max}}$ for the free-floating canard with a reflexed trailing edge of 0.5, the set of equations can be solved to yield a stable, trimmed design with a wing C_L of 1.8 at a flap angle of 45 deg. The resulting tail volume coefficient is

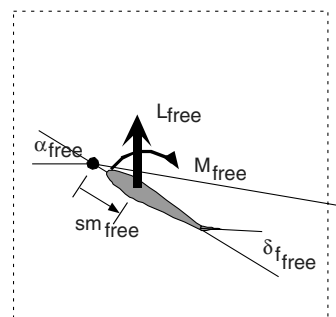


Fig. 25 Close-up view of the forces and moments on the free-floating canard.

$$\bar{d}\bar{S} > 0.0107\pi^2 \quad (38)$$

and the swept radius is

$$R_s = c_w \times \max\left(\bar{d} + \frac{1}{4}\bar{c}, \bar{S} + \frac{3}{4}\right) \quad (39)$$

The reason for the two terms is due to the possibility that the canard sticks farther forward than the wing extends back.

The stall characteristics of the free-floating canard configuration require some discussion; at stall, the main wing loses lift, however, the free-floating canard does not. The main wing also sees an increase in nose down pitching moment at stall, due to the separated flow off the back of the main wing section. The loss of lift on the main wing tends to pitch the nose upward, increasing the stall, but the increase in pitching moment tends to pitch the nose down, decreasing the stall. The canard itself contributes nothing but its steady lift, which does not change during the stall. The main wing must increase its pitching moment faster than the moment generated by the loss of lift and the moment arm to the pivot point.

The original design of the Ascender did not achieve this balance and suffered from a divergent stall that pitched the aircraft over onto its back. Eventually, the designers realized the problem and fixed the aircraft main wing (as the canard played no role in the transient).

VII. Configuration Results

The analysis of the four different possible configurations for trim and stability shows that only two configurations are viable: the conventional tail and the free-floating canard. The normal canard cannot be both stable and trimmed with a trailing-edge flap, and the flying wing needs to reflex the trailing edge for stability, thus reducing the attainable maximum lift coefficient.

The results of the analysis are summarized in Table 1, including the normalized tail volume [Eq. (21) and (38)] and the swept radius [Eq. (22) and (39)]. The tail volume requirement for the free-floating canard is almost double that of the conventional configuration. In addition, the free-floating canard is mechanically more complicated, with another pivot point and an additional flap on the trimming surface. The main benefit of the free-floating canard is a much reduced swept radius, which might allow the wing not to overhang the hulls. This is due to the canard/wing combination being more centered about the pivot point.

Upon completing the calculations, however, the actual swept radius is only marginally smaller, thus canceling the free-floating canard advantage. The Atlantis was fitted with a wingsail and conventional tail layout, as shown in Fig. 16.

VIII. Conclusions

This paper demonstrates the design of a wing section suitable for a wingsail on an autonomous wind-propelled marine surface vehicle. The design criteria for the wing are challenging: low Reynolds number, large lift coefficients, and a requirement of symmetric geometry to sail to both port and starboard.

Using two CFD codes, PANDA and XFOIL, a section was designed that meets all of the criteria. The resulting section is a very thick symmetric section, with a 21% thickness-to-chord ratio, that is capable of reaching a $C_{L_{\max}}$ of 1.8 at a Reynolds number of 229,000. To reach this high-lift coefficient, the section has a plain narrow-chord flap that is only 13% of the wing chord.

Table 1 Configuration analysis results

Configuration	Tail volume	Swept radius
Conventional	$\bar{d}\bar{S} > 0.00528\pi^2$	$R_s = c_w[\bar{d} + \frac{3}{4}\bar{c}]$
Canard	Unstable	n/a
Flying wing	Low $C_{L_{\max}}$	n/a
Free-floating canard	$\bar{d}\bar{S} > 0.0107\pi^2$	$R_s = c_w \times \max(\bar{d} + \frac{1}{4}\bar{c}, \bar{S} + \frac{3}{4})$

A grid search was performed to find the optimum wing-to-flap chord ratio to maximize the lift/drag ratio. The section requires trip strips to transition the boundary layer from laminar to turbulent. Some questions remain as to the real-world efficacy of the trip strips, which will have to be validated experimentally.

A similar design was performed for the tail that demonstrates a maximum lift coefficient of 0.75 at a Reynolds number of 44,000, which corresponds to boat speeds of approximately 5 kt in a 3–6 kt breeze. Using the results of the section design, and a combination of thin airfoil and simplified lifting line theory, this paper extends the analysis performed in [22] to account for finite aspect ratios and downwash/upwash effects.

Four different wing/tail configurations are evaluated for passive stability and the ability to trim a high C_L . They are 1) conventional (tail behind wing), 2) canard (tail in front of wing), 3) swept/tapered flying wing, and 4) a free-floating canard, where the canard surface itself has a flap and pivot point to allow it to hold a constant angle of attack to the incoming flow.

The canard and the flying wing are both found to be unable to meet the passive stability and trim criteria. The canard can only be stable at one design point, and the flying wing can be stable but cannot trim the design load due to reflexing the trailing edge with the flap for trim.

Both the conventional and free-floating canard can be made to meet the design criteria, however, the free-floating canard is mechanically much more complicated and requires a larger trimming surface (due to lower efficiency). Thus, the conventional configuration was chosen.

This wing has been built and experimentally tested on the Atlantis project and shows great potential for autonomous wind-propelled marine surface vehicles. It has demonstrated both passive stability, holding a constant angle of attack relative to the wind, and the ability to hold a high C_L while under sail.

Acknowledgments

The initial part of this research was conducted under a birdseed grant from the Stanford Office of Technology Licensing. The author gratefully acknowledges both the Office of Technology Licensing and the Principal Investigator, Bradford Parkinson, of Stanford University for support and sharing the data.

References

- [1] Pascoal, A., Olivera, P., and Silvestre, C., "Robotic Ocean Vehicles for Marine Science Applications: The European ASIMOV Project," *OCEANS 2000 MTS/IEEE Conference and Exhibition*, Vol. 1, Marine Technology Society, Washington, D.C., 2000, pp. 409–415.
- [2] Elkaim, G., "Atlantis Project: A GPS-Guided Wing-Sailed Autonomous Catamaran," *Navigation*, Vol. 53, No. 4, 2006, pp. 237–247.
- [3] Gebre-Egziabher, D., Elkaim, G. H., Powell, J. D., and Parkinson, B. W., "A Gyro-Free, Quaternion Based Attitude Determination System Suitable for Implementation Using Low-Cost Sensors," *Proceedings of the IEEE Position Location and Navigation Symposium*, Inst. of Electrical and Electronics Engineers, New York, 2000, pp. 185–192.
- [4] Juang, J.-N., *Applied System Identification*, Prentice-Hall, Upper Saddle River, NJ, 1994.
- [5] Elkaim, G., "System Identification for Precision Control of a Wingsailed GPS-Guided Catamaran," Ph.D. Thesis, Stanford Univ., Stanford, CA, 2001.
- [6] Encarnacao, P., Pascoal, A., and Arcaç, M., "Path Following for Autonomous Marine Craft," *5th IFAC Conference on Maneuvering and Control of Marine Craft*, International Federation of Automatic Control, 2000, pp. 117–22.
- [7] Fossen, T., *Guidance and Control of Ocean Vehicles*, Wiley, New York, 1994.
- [8] Breivik, M., and Fossen, T. I., "Path Following for Marine Surface Vessels," *OCEANS '04 MTS/IEEE Techno-Ocean '04*, Vol. 4, Inst. of Electrical and Electronics Engineers, New York, Nov. 2004, pp. 2282–2289.
- [9] Van Zwielen, T., "Dynamic Simulation and Control of an Autonomous Surface Vehicle," Ph.D. Thesis, Florida Atlantic Univ., Boca Raton, FL, 2003.

- [10] Marchaj, C. A., *Sail Performance: Techniques to Maximize Sail Power*, International Marine, Camden, ME, 1996.
- [11] Selig, M. S., Donovan, J. F., and Fraser, D. B., *Airfoils at Low Speeds*, H. A. Stokley, Virginia Beach, VA, 1989.
- [12] Birchill, J., "Windform Sail," *Ancient Interface II, Proceedings of the Second AIAA Symposium on the Aer/Hydronautics of Sailing*, Vol. 9, AIAA Lecture Series, AIAA, Los Angeles, 1970, pp. 59–73.
- [13] Ross, J. C., "Aerodynamic Design of a Rigid-Wing Sail for a C-Class Catamaran," *The Ancient Interface XVIII, Proceedings of the Eighteenth AIAA Symposium on the Aer/Hydronautics of Sailing*, Vol. 35, AIAA Lecture Series, AIAA, Reston, VA, 1989, pp. 17–27.
- [14] Kroo, I., and McGeer, T., "Optimization of Canard Configurations," *13th ICAS Congress*, International Council of the Aeronautical Sciences 82-6.8.1, 1982.
- [15] McGeer, T., and Kroo, I., "A Fundamental Comparison of Canard and Conventional Configurations," *Journal of Aircraft*, Vol. 20, No. 11, 1983, pp. 983–992. doi:10.2514/3.48202
- [16] Drela, M., "A New Transformation and Integration Scheme for the Compressible Boundary Layer Equations, and Solution Behavior at Separation," MIT Press, Cambridge, MA, Massachusetts Inst. of Technology Gas Turbine Lab. Rept. 172, May 1983.
- [17] Drela, M., "XFOIL: An Analysis and Design System for Low Reynolds Number Airfoils," *Conference on Low Reynolds Number Airfoil Aerodynamics*, Univ. of Notre Dame Press, South Bend, IN, June 1989.
- [18] Drela, M., and Giles, M., "Viscous-Inviscid Analysis of Transonic and Low Reynolds Number Airfoils," *AIAA Journal*, Vol. 25, No. 10, 1987, pp. 1347–1355. doi:10.2514/3.9789
- [19] Giles, M., and Drela, M., "Two-Dimensional Transonic Aerodynamic Design Method," *AIAA Journal*, Vol. 25, No. 9, 1987, pp. 1199–1206. doi:10.2514/3.9768
- [20] McCormick, B., *Aerodynamics, Aeronautics, and Flight Mechanics*, Wiley, New York, 1979.
- [21] Shevell, R. S., *Fundamentals of Flight*, Prentice-Hall, Englewood Cliffs, NJ, 1983.
- [22] Fekete, G., and Newmann, G., "Design and Testing of a Sailboat with Self-Trimming Wingsail," *Canadian Aeronautics and Space Journal*, Vol. 29, No. 2, June 1983, pp. 121–130.
- [23] Glauert, H., *The Elements of Aerofoil and Airscrew Theory*, Cambridge Univ. Press, New York, 1983.
- [24] Munk, M. M., "General Biplane Theory," NACA Rept. 151, 1922.